Synthesis, Characterization and Quantum Chemical Studies of Inhibition Ability of Novel 5-Nitro Isatin Derivatives on The Corrosion of Carbon Steel in Sea Water

Rehab M. Kubba, Suaad M. H. Al-Majidi, Athraa H. Ahmed*
Department of Chemistry, College of Science, University of Baghdad, Baghdad, Iraq

Abstract

This research includes synthesis of new 5-Nitro isatin derivatives starting from 5-Nitro-3-(ethyl imino acetate)-2-oxo indole (1) namely 5-nitro-3-[(imino acetyl) semicarbazide]-2-oxo indole (2); 5-nitro-3-[(imino acetyl) phenylsemicarbazide]-2-oxo indole (3); 5-nitro-3-[(imino acetyl) thiosemicarbazide]-2-oxo indole (4); 5-nitro-3-[(iminoacetyl) phenylthiosemi carbazide]-2-oxo indole (5); 5-nitro-3-[(methyl imino)-4H-1, 2, 4-triazol-5-ol-3-yl]-2-oxo indole (6); 5-nitro-3-[(methyl imino) 4-phenyl-1, 2, 4-triazol-5-ol-3-yl]-2-oxo indole (7); 5-nitro-3-[(methyl imino) 4-phenyl-1, 2, 4-triazol-5-thiol-3-yl]-2-oxo indole (8) and 5-nitro-3-[(methyl imino) 4H-1, 2, 4-triazol-5-thiol-3-yl]-2-oxo indole (9). The derivatives were characterized using FTIR, ^{1}HNMR, ^{13}CNMR and C.H.N.S analysis with the measurement of some physical properties.

Quantum mechanical method of the Density Functional Theory (DFT) of B3LYP with a level of 6-311++G (2d, 2p) were used to calculate the geometrical structure, physical properties, and inhibition efficiency parameters, at the equilibrium geometry in four media (vacuum, DMSO, ETOH and H_2O). The theoretical results showed that compound (7) was the best corrosion inhibitor among the others. Finally, potentiodynamic polarization studies showed that the compound (7) was a mixed type inhibitor. The adsorption of this compound on a carbon steel surface from sea water obeyed the Langmuir adsorption isotherm. The decrease in the inhibition efficiency with the increase in temperature and the low negative values of $\Delta H°ads$ suggest predominant physisorption of the prepared compound (7) on the carbon steel surface. The surface morphology of the carbon steel before and after inhibition was studied using SEM (Scanning Electron Microscopy) and AFM (Atomic Force Microscopy) techniques.

Keywords-5- nitro isatin, 1, 2, 4-triazolederivatives, corrosion inhibitors, quantum chemical calculations, electrochemical measurements

تحضير، تشخيص ودراسة كيمياء الكم لقابلية تثبيط بعض مشتقات 5– نايتروايساتين الجديدة لتآكل حديد الصلب الكربوني في ماء البحر

رحاب ماجد كبة ، سعاد محمد حسين الماجدي، عذراء حكمت أحمد*
قسم الكيمياء، كلية العلوم جامعة بغداد، بغداد، العراق

الخلاصة

يتضمن البحث تحضير مشتقات جديدة من 5– نايترو–3–(اثيل امينواستيت)–2–اوكسواندول **(1)** وهي 5– نايترو –3– [(امينو استيل) سيميكاربازيد] –2– اوكسو اندول **(2)**، 5– نايترو –3– [(امينو استيل)

_____

*Email: hekmat@yahoo.com

فنيل سيميكاربازايد] -2- اوكسو اندول **(3)**، 5- نايترو -3- [(امينو استيل) ثايو سيميكاربازايد] -2-
اوكسو اندول **(4)**، 5- نايترو -3- [(امينو استيل) فنيل ثايو سيميكاربازايد] -2- اوكسو اندول **(5)**، 5-
نايترو -3- [(مثيل امينو)-H4 -4،2،1-ترايزول-5- اول-3- يل]-2- اوكسو اندول **(6)**، 5-نايترو
-3- [(مثيل امينو)-4-فنيل-4,2,1-ترايزول-5- اول-3- يل]-2- اوكسو اندول **(7)**, 5-نايترو -3-
[(مثيل امينو)-4-فنيل-4,2,1-ترايزول-5- ثايول-3- يل]-2- اوكسو اندول **(8)** و 5-نايترو -3-
[(مثيل امينو)-H4 -4،2،1-ترايزول-5- ثايول-3- يل]-2- اوكسو اندول **(9)**. وتم تشخيص هذه
المشتقات باستخدام مطيافية FTIR و H–NMR¹ و ¹³C–NMR وتحليل عناصر C.H.N.S مع قياس
بعض الخصائص الفيزيائية.

وقد تم استخدام طريقة حسابات ميكانيك الكم وفق نظرية دوال الكثافة (DFT) عند المستوى 6– B3LYP
(2d,2p) G++311) لحساب البنية الهندسية والخصائص الفيزيائية ومعاملات كفاءة التثبيط والتي تمت
دراستها عند الشكل الهندسي المتوازن في أربعة أوساط (الفراغ والمذيبات DMSO و EtOH و H₂O).
أظهرت نتائج الحسابات النظرية أفضلية المركب **(7)** كمثبط للتآكل من بين المشتقات الأخرى. وأخيرًا،
أظهرت دراسة الاستقطاب المجهادي أن المركب **(7)** يسلك سلوك مثبط مزدوج وأن امتزازه على سطح حديد
الصلب الكربوني يطيع ايزوثيرم امتزاز لنكماير. وان كفاءة التثبيط تقل بأرتفاع درجة الحرارة اضافة الى أن
القيم الواطئة لانثالبي الامتزاز ΔH_ads تؤكد عملية الامتزاز الفيزياوي للمركب **(7)** على سطح حديد الصلب
الكربوني. تمت دراسة التشكل السطحي لحديد الصلب الكربوني قبل وبعد التثبيط باستخدام تقنية مجهر المسح
الإلكتروني (SEM) وتقنية مجهر القوة الذرية (AFM).

Introduction

Isatin is the reference compound of an important class of nitrogen-containing aromatic heterocyclic compounds, which have been found in many plants and tissue [1].
1,2,4-triazoles derivatives have a broad spectrum of biological activity and this is applied especially for heteryl condensing derivatives-1,2,4-triazoles substituted by benz-thiazole, benz-oxazole, thiazole fragments which exhibit a pronounced anti-inflammatory, antibacterial, anti-tuberculosis, analgesic and other properties [2].

Quantum chemical calculations had been used to study the reaction mechanism and to solve chemical ambiguities. This is a useful approach to investigate the reaction mechanism of the inhibitor molecule and the metal surface. The structural and electronic parameters of the inhibitor molecule can be obtained by theoretical calculations using the computational methodologies of quantum chemistry [3].

Corrosion inhibitors are chemicals that react with a metallic surface or the environments the metal surface is exposed to an act to protect the metal against corrosion [4]. Most organic compounds having hetero atoms (N,O,S) in their aromatic structure have been successfully used as corrosion inhibitors [5]. The heterogeneous organic compounds having higher basicity and electron density on the hetero atoms usually have the tendency to resist corrosion.

The aim of the present work is to prepare new 5-nitro isatin derivatives, and studying their corrosion inhibition ability theoretically in four media (vacuum, DMSO, EtOH and water) for choosing the expected best corrosion inhibitor by calculating parameters of the quantum mechanical inhibition efficiency using DFT [6-311/ B3LYP++G (2d, 2p)] method. The best expected inhibitor was compound (7). And to confirm the inhibition ability of a compound (7), it was studied experimentally as a corrosion inhibitor of carbon steel in sea water by using the potentiodynamic polarization, SEM and AFM measurements.

Experimental part

1. Synthesis of 5-nitro-3-[(iminoacetyl) phenylthiosemi carbazide]-2-oxo indole (2), 5-nitro-3-[(iminoacetyl) phenylsemicarbazide]-2-oxo indole (3), 5-nitro-3-[(imino acetyl)semicarbazide]-2-oxo indole (4) and 5-nitro-3-[(iminoacetyl)thiosemicarbazide]-2-oxo indole (5) [6].

A mixture of 5-Nitro-3-(Ethyl imino acetate)-2-oxo indole (1)[7](3 g, 0.0106 mol) with (0.0106 mol) semicarbazide, phenylsemicarbazide, thiosemicarbazide, or phenylthiosemicarbazide respectively and (0.93 g, 0.0106 mol) of sodium acetate in 30 ml absolute ethanol were refluxed for (14-16) hours. The mixture was poured on ice water filtered, dried and recrystallized from absolute ethanol to give crystals. The physical properties of products are listed in Table 1.

2. Synthesis of 5-nitro-3-[(methylimino)-4H-1,2,4-triazol-5-ol-3-yl]-2-oxo indole(6), 5-nitro-3-[(methylimino) 4-phenyl-1,2,4-triazol-5-ol-3-yl]-2-oxo indole(7), 5-nitro-3-[(methylimino) 4-phenyl-1,2,4-triazol-5-thiol-3-yl]-2-oxo indole (8) and 5-nitro-3-[(methylimino) 4H-1,2,4-triazol-5-thiol-3-yl]-2-oxo indole (9) [6].

In round bottom flask (0.0032 mol) of compounds (2, 3, 4 or 5) was refluxed with (4N) aqueous sodium hydroxide solution for (10-12) hours. After cooling, poured on ice water, and neutralized by gradual addition of (1:1) hydrochloric acid. The precipitate was filtered, dried and recrystallized from ethanol. The physical properties and FTIR of compounds (6-9) are listed in Table 1.

Preparation of solutions
Blank solution
35 g of NaCl was dissolved in distilled water, transferred to 1L volumetric flask, and 2ml of DMSO was added, then the volume completed to 1L with distal water.

5-nitro-3-[(methylimino) 4-phenyl-1,2,4-triazol-5-ol-3-yl]-2-oxo indole (7)solutions
Three concentrations of (5, 10 and 20) ppm were prepared by dissolving (0.005, 0.01 and 0.02) g, of compound **(7)** respectively, in 2ml DMSO, transferred to a volumetric flask of 1L. Then 35g of NaCl was added to each concentration after dissolving in distilled water before completing the volume to 1L.

Electrochemical measurements
Potentiostatic polarization study
The potentiostat set up includes a Host computer, thermostat, magnetic stirrer, Mat lab (Germany, 2000), potentiostat, and galvanostat. The corrosion cell is (1L) capacity made of Pyrex consist of two bowls internal and external. The electrochemical corrosion cell is a three electrodes cell containing a working electrode carbon steel with $1cm^2$ surface area used to determine the potential of working electrode according to the reference electrode, a platinum auxiliary electrode with length (10cm) and a silver-silver chloride (Ag/AgCl, 3.0M KCl) reference electrode. The working electrode was immersed in the test solution for 30 min. to establish state open circuit potential (E_{ocp}), then electrochemical measurements were performed in potential range of (±200) mV. All tests were carried out at temperature of (298-318) K by controlling the cell temperature using a cooling heating circulating water bath.

Results and discussion
Synthesis of 5-Nitro isatin derivatives
Ester derivative (1) was converted to semicarbazide (4), phenylsemicarbazide (3), thiosemicarbazide (5) and phenylthiosemicarbazide (2) derivatives by reaction with semicarbazide, phenylsemicarbazide, thiosemicarbazide and phenylthiosemicarbazide respectively in absolute ethanol as a solvent, Equation 1.
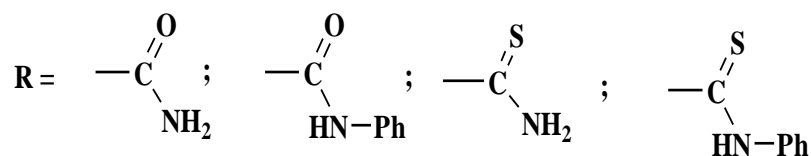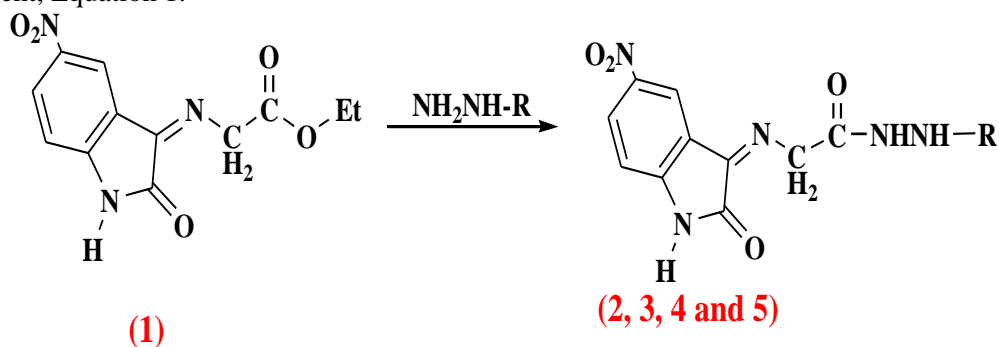
Equation (1).

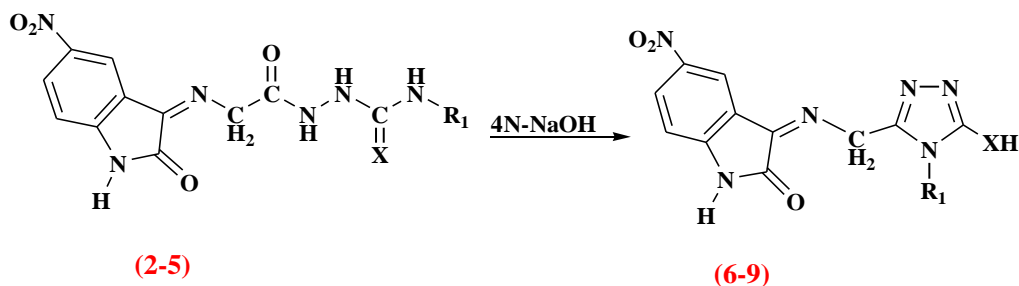The mechanism of this reaction [8] is shown in Scheme 1.
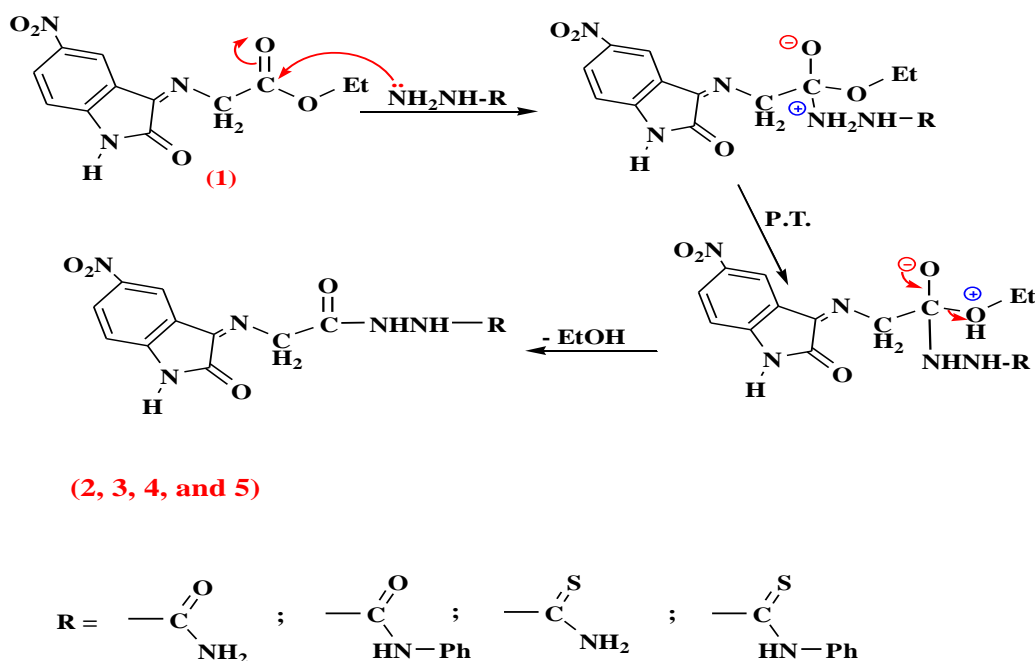
Scheme (1)

The physical properties of compounds (2, 3, 4 and 5) are listed in Table 1. FTIR spectrum of compound (4) showed the appearance of the absorption band for $\upsilon(NH_2)$ group asymmetric at (3434) cm^{-1} and symmetric at (3294) cm^{-1}, and $\upsilon(N-H)$ group stretching band at (3247) cm^{-1}. Also showed $\upsilon(C=O)$ bands at (1713, 1706) cm^{-1} of amide. FTIR spectrum of compound (3) showed an appearance of absorption band at (3244) cm^{-1} for $\upsilon(N-H)$ and (1695, 1666) cm$^{-1}\upsilon(C=O)$ of amide [9]. While in compound (5) showed absorption band at (3473) cm^{-1} asym. (3373) cm^{-1} sym. for $\upsilon(NH_2)$, absorption band at (3249) cm^{-1} for $\upsilon(N-H)$ and (1697, 1654)cm$^{-1}\upsilon(C=O)$ of amide also showed absorption band at (1259) for $\upsilon(C=S)$ group. Finally FTIR spectrum of compound (2) showed absorption band at (3244) cm^{-1} for $\upsilon(N-H)$, $\upsilon(C=O)$of amide at (1695, 1666) cm^{-1} and (1292) cm^{-1} for $\upsilon(C=S)$. FTIR spectral data are listed in Table-1.

^{1}H-NMR (DMSO-d_6) spectrum of compound (4) showed signal at δ= 3.82 ppm due to (s, 2H, =N-C$\underline{H}_2$) protons, showed multiple signal at δ= (7.19-8.19) ppm due (C-H) protons of benzene ring also absorption band at δ= (8.52) for (s, 2H, N$\underline{H}_2$), signal at 9.72 for (s, 2H, O=C-N$\underline{H}$) and singlet signal at δ= (10.71) ppm due to (N-H indole) proton. Results of ^{1}HNMR Spectra for compound (4) are listed in Table 2.^{13}C-NMR spectral data of compound (4) are listed in Table 3.

Treatment of compounds (2-5) with alkaline medium (4N) NaOH solution affords intramolecular cyclization to give the hydroxytriazole (6), phenylhydroxy triazole (7), thiotriazole (8) and phenylthio triazole (9) respectively, Equation 2.

when X= S   ;   R$_1$= H or Ph
when X =O   ;   R$_1$= H or Ph

Equation (2)

The mechanism of reaction involved nucleophilic attack lead to cyclization [10] as shown in Scheme 2.
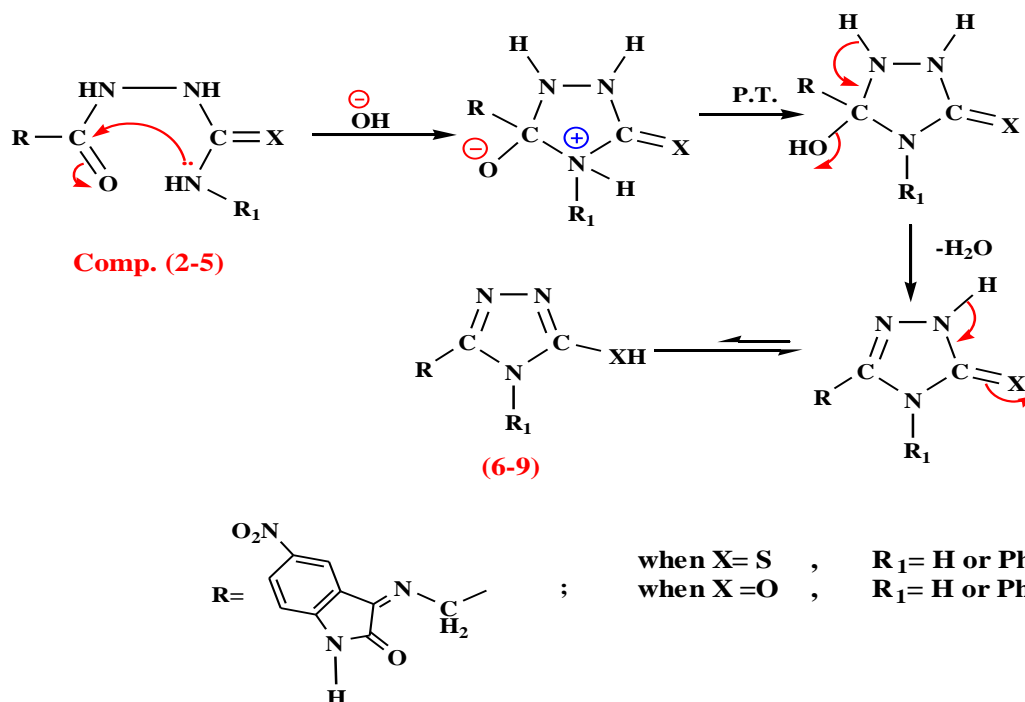
Scheme (2)

The physical properties of compounds (6-9) are listed in Table-1. These compounds were identified from FTIR spectra, all spectral data showed the presence of absorption band of υ(C=N) group at about (1620-1629) cm^{-1} with appearance of υ(O-H) for compound (6 and 7) at (3352, 3454) cm^{-1} respectively, also show υ(S-H) at (2550-2700) cm^{-1} for compounds (8 and 9) the results are listed in Table 1.

^{1}HNMR spectrum for compound (7) showed signals at 4.33 due to(=N-C$\underline{H}_2$-) protons, absorption band at 6.89 due to proton of (-OH), multiple signal at 6.97-7.84 due to aromatic ring protons, also signal at 10.29 for N-$\underline{H}$ tautomeric form and signal at 11.64 due to (-NH indole) proton. Results of ^{1}HNMR Spectra for compound (7) are listed in Table-2.

The ^{13}C-NMR spectral data of compound (7) are listed in Table-3. The C.H.N analysis for compound (7) is listed in Table -4.

Table 1-Physical properties and FTIR spectral data of the synthesized compounds (2-9)

Com No.	Physical Properties				Major FTIR Absorption (cm^{-1})			
	Structure	M.P. °C	Yield %	Color	υ(N-H)	υ(C-H) aromatic	υ(C-H) aliphatic.	υ(C=O) amide
2		117-118	75	Brown	3244	3068	2920 2850	1695 1666
3		114-115	85	Brown	3244	3068	2920 2850	1695 1666
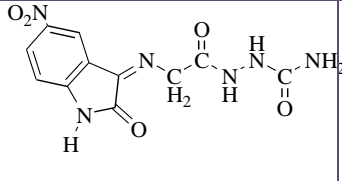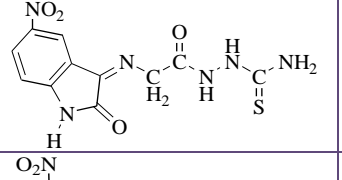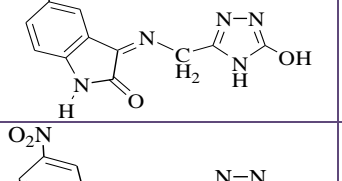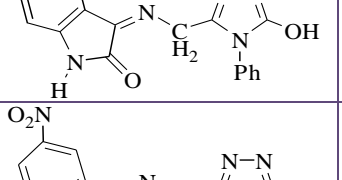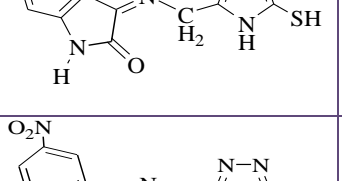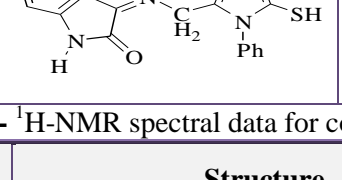
No.	Structure	mp (°C)	Yield %	Color				
4		108-110	84	Brown	3247	3074	2914 2884	1713 1706
5		119-120	80	Brown	3249	3080	2997 2937	1697 1654
6		191-193	75	Dark brown	3251	3076	2923 2883	1699
7		208-210	80	Dark brown	3224	3081	2966 2925	1693
8		197-200	71	Black	3282	3068	2898	1720 1697
9		234-237	85	Black	3336	3066	2880	1681

Table 2- ^{1}H-NMR spectral data for compounds (4 and 7)
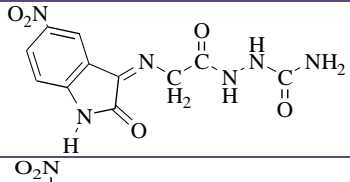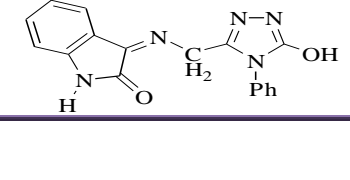
Com. No.	Structure	^{1}HNMR spectral data (δ, ppm)
4		3.82 (s, 2H, =N-C$\underline{H}_2$); 7.19-8.19 (m, 3H,Ar-$\underline{H}$); 8.52 (s, 2H, N$\underline{H}_2$); 9.72 (s, 2H, O=C-N$\underline{H}$); 10.71 (N-H indole).
7		4.33 (s, 2H, =N-C$\underline{H}_2$-); 6.89 (s, 1H, O-$\underline{H}$); 6.97-7.84 (m, 8H, Ar-$\underline{H}$); 10.29 (s, 1H, N-$\underline{H}$ tautomeric form); 11.64 (s, 1H, N-$\underline{H}$ indole).

Table 3-^{13}C-NMR spectral data for compounds (4 and 7)
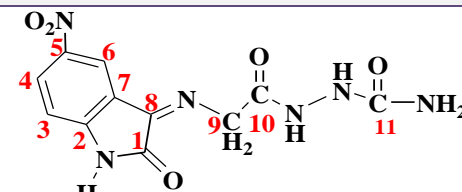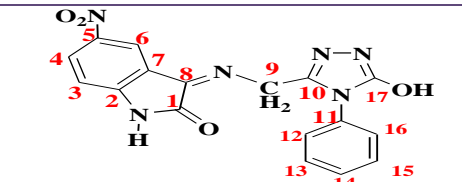
Com. No.	Structure	^{13}CNMR spectral data (δ, ppm)
4		64 (C9); 126-135 (C2, 3, 4, 5, 6, 7); 156 (C8); 161 (C1, 10); 169 (C11).
7		70 (C9); 111-121 (C2, 3, 4, 5, 6, 7, 11, 12, 13, 14, 15, 16); 155 (C8, 10, 17); 163 (C1).

Table 4-The C.H.N analysis for compound (7)

Com. No.	Molecular Formula	Calculated (%)			Found (%)		
		C	H	N	C	H	N
7	$C_{17}H_{12}N_6O_4$	56.05	3.32	23.07	55.00	3.31	22.89

Quantum chemical calculations

The structural nature of the organic inhibitors and their inhibition mechanism were described by density functional theory (DFT). The inhibition efficiencies of compounds (6-9)were investigated by the theoretical corrosion inhibition parameters such as energy of the highest occupied molecular orbital (E_{HOMO}) and energy of the lowest unoccupied molecular orbital(E_{LUMO}), energy gap (ΔE) between E_{HOMO} and E_{LUMO}, dipole moment (μ), electronegativity (χ), electron affinity (A), global hardness (η), softness (σ), ionization energy (IE), global electrophilicity (ω), the fraction of electrons transferred (ΔN) and the total energy (E_{tot}) [11].

Molecular geometry

The compound was built using Chem Draw of MOPAC program. Gaussian 09 packages were used for calculating the equilibrium geometry [12]. The corresponding geometry in the vacuum phase was fully optimized using DFT (Density Functional Theory) which was carried out using a basis set of (B3LYP) with a 6-311++G (2d, 2p) level of the theory [13,14]. Also, the equilibrium geometry was calculated in three solvent media (ETOH, DMSO, and H_2O). Figure-1 shows the numbering of atoms of compound (7).
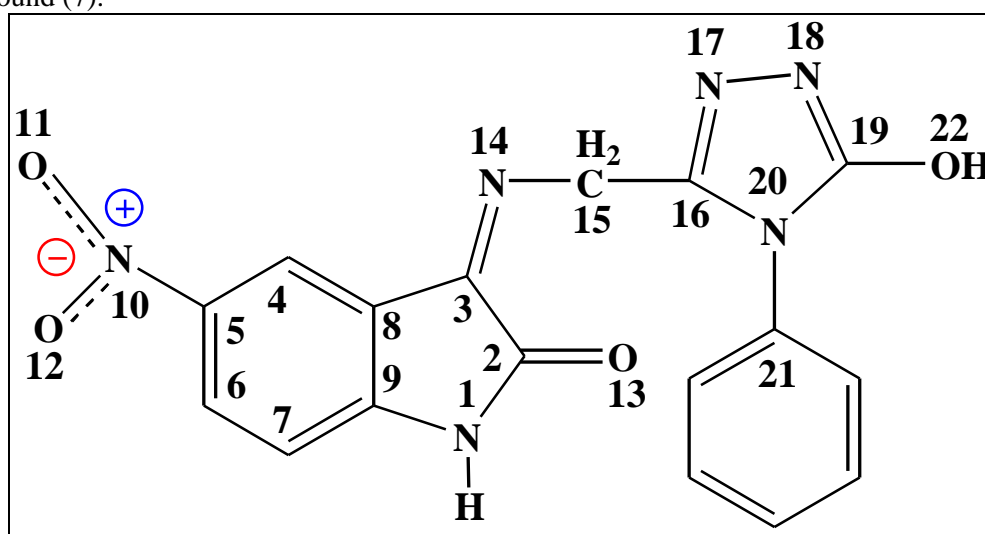
Figure 1-The numbering of atoms for compound (7).

The computational of the structural parameters such as bond angles, bond distances, and dihedral angles were assayed. The longest bond length was observed for C2-C3 (1.536 A°). The shortest bond

length was observed for N1-H (1.009 A°). The bond angles were getting between (27.920 A°) for O11N10O12 and (131.268 A°) for C3C8C4. The values of the dihedral angles (trans & cis) indicated non-planar compound with asymmetry of C_1 [all cis dihedral angles are higher or lower than 0.0 degree and the all trans dihedral angles are higher or lower than 180.0], Table-5, Figure-2a.

The functionalize adsorption part is located at the planer part of the molecule, Figure-2b.

Table 5-Geometrical structure for compound (7) in the media of (vacuum, ETOH, DMSO, and H_2O) as calculated by using DFT method.

Description Bond length	Bond length (Å)	Description angle	Angle (deg)	Description Dihedral angle	Dihedral angle (deg)
N1-C2	1.390	C2N1H	120.886	N1C2C3C8	2.259
N1-C9	1.397	N1C2C3	105.479	N1C2C3N14	-178.046
N1-H	1.009	N1C2O13	125.281	HN1C2O13	16.128
C2-C3	1.536	C2C3C8	105.076	C2C3C8C4	179.063
C2=O13	1.211	C2C3N14	129.559	C2C3C8C9	0.109
C3-C8	1.469	C8C4C5	117.296	C3C8C9C7	178.977
C3-N14	1.268	C4C5C6	122.256	C3C8C9N1	-2.481
C4-C5	1.396	C6C5N10	118.688	C8C4C5C6	0.206
C4-C8	1.382	C5C6C7	120.290	C8C4C5N10	-179.801
C5-C6	1.396	C6C7C9	117.698	C4C5C6C7	-0.506
C5-N10	1.458	C3C8C9	107.952	N10C5C6C7	179.501
C6-C7	1.392	C3C8C4	131.268	C2C3N14C15	-1.343
C7-C9	1.389	C7C9N1	128.712	C3N14C15C16	-79.177
C8-C9	1.407	C5N10O11	117.817	N14C15C16N17	-11.093
N10-O11	1.230	O11N10O12	27.920	C15C16N17N18	-175.759
N10-O12	1.231	C3N14C15	120.491	C16N17N18C19	0.575
N14-C15	1.463	N14C15C16	111.119	N17N18C19N20	-0.462
C15-H2	1.090	N14C15H2	111.716	N18C19N20C21	-175.637
C15-C16	1.504	C15C16N17	125.414	------	------
C16-N17	1.300	C16N17N18	107.782	------	------
N17-N18	1.400	N17N18C19	106.169	------	------
N18-C19	1.297	N18C19N20	112.559	------	------
C19-N20	1.371	C19N20C21	127.126	------	------
N20-C21	1.429	N20C19O22	120.646	------	------
C19-O21	1.342	N18C19O22	126.785	------	------

Global molecular reactivity:

Frontier orbital theory is used in predicting adsorption centers of the inhibitor responsible for the reaction metal surface/molecule [15]. The calculated quantum chemical parameters related to the inhibition efficiency of the studied molecule are collected in Tables-(6a, 6b). They are calculated according to the following equations:

IP (Ionization potential) = $-E_{HOMO}$ (3)

EA (Electron affinity) = $-E_{LUMO}$....   (4)

H (Hardness) = (IE - EA)/ 2…   (5)

X (Electro negativity) = (IE + EA)/ 2 ..   (6)

The Global softness (S) is the inverse of the global hardness.

S (global softness) = 1/ η .   (7)

The Global electrophilicity index (**ω**) introduced by Parr [16], using for calculating the electronegativity and chemical hardness parameters, Equation 8:

$\quad$ Global electrophilicity index (ω) = $(-\chi)^2/2\eta = \mu^2/2\eta$...   (8)

The fraction of electrons transferred (ΔN) from an inhibitor to carbon steel surface was also calculated using theoretical χ_{Fe} and η_{Fe} values for mild steel of 7.0 eV mol^{-1} and 0.0 eV mol^{-1}, respectively. The number of transferred electrons (ΔN) was also calculated [17] by using Equation (9).

ΔN (Electron transferred) = $(\chi_{Fe} - \chi_{inhib.})/[2(\eta_{Fe} + \eta_{inhib.})]$ (9)

$\quad$ The calculated quantum chemical parameters in the vacuum, ETOH, DMSO and H$_2$O had shown a good effect for increasing the efficiency inhibition for compound (**7**), Tables (6a, 6b). Figure-2 showed the geometry optimization of the studied compound in the vacuum including HOMO and LUMO density distributions. The HOMO mainly located on the 1, 2, 4-tiazole moiety, this would indicate that the preferred actives sites for an electrophilic attack are located within the region around the nitrogen atoms. Moreover, the electronic density of LUMO was distributed at the aromatic ring and ring of isatin moiety.

(a)	(a)
(b)	(b)
HOMO	**LUMO**
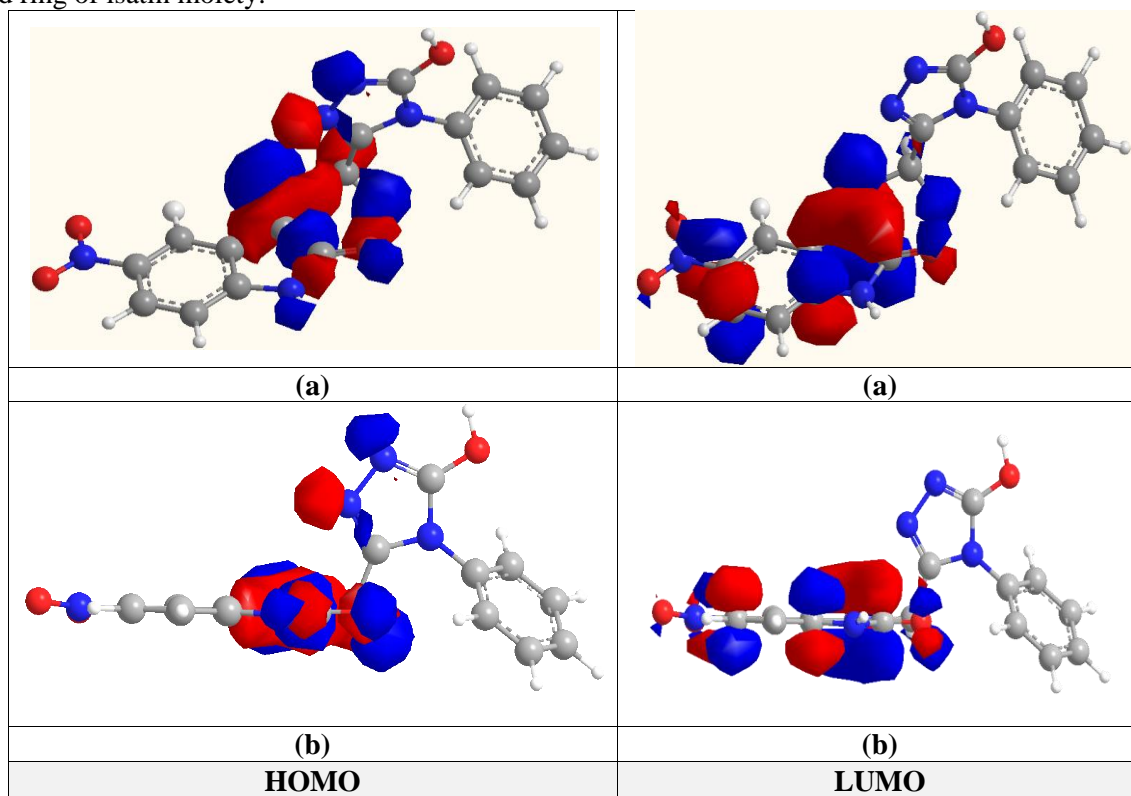
Figure 2(a)-The Frontier Molecular Orbital density distributions of the studying 5-Nitro isatin derivative, (**b**) The most planar region in the molecule. [Red color: negatively charged lobe; blue color: positive charge lobe].

Table 6(a)-DFT calculations for some physical properties of the inhibitor molecules (**6-9**) at their equilibrium geometries.

Inhib. Media	P. G.	M. formula	E$_{HOMO}$ (eV)	E$_{LUMO}$ (eV)	ΔE$_{LUMO-HOMO}$ (eV)	μ (Debye)	E$_{total}$ (eV)
(6)							
Vacuum	C$_1$		-6.568	-3.471	3.096	4.990	-28670.0
ETOH	C$_1$	C$_{11}$H$_8$N$_6$O$_4$	-6.738	-3.141	3.597	6.701	-28670.7
DMSO	C$_1$		-6.744	-3.132	3.612	6.760	-28670.7

H$_2$O	C$_1$		-6.747	-3.128	3.619	6.787	-28670.7
(7)							
Vacuum	C$_1$	C$_{17}$H$_{12}$N$_6$O$_4$	-6.740	-3.170	3.570	7.806	-34958.7
ETOH	C$_1$		-6.963	-3.147	3.815	10.402	-34959.4
DMSO	C$_1$		-6.964	-3.149	3.814	10.501	-34959.5
H$_2$O	C$_1$		-6.984	-3.151	3.833	10.546	-34959.5
(8)							
Vacuum	C$_1$	C$_{11}$H$_8$N$_6$O$_3$S	-6.608	-3.773	2.835	7.309	-37458.0
ETOH	C$_1$		-6.780	-3.425	3.354	9.458	-37458.8
DMSO	C$_1$		-6.786	-3.418	3.367	9.528	-37458.8
H$_2$O	C$_1$		-6.788	-3.414	3.374	9.561	-37458.8
(9)							
Vacuum	C$_1$	C$_{17}$H$_{12}$N$_6$O$_3$S	-6.328	-3.207	3.120	7.468	-43746.7
ETOH	C$_1$		-6.477	-3.172	3.305	9.873	-43747.4
DMSO	C$_1$		-6.486	-3.174	3.311	9.963	-43747.4
H$_2$O	C$_1$		-6.489	-3.175	3.314	10.006	-43747.4

Table 6(b)-Quantum chemical parameters for inhibitor molecules **(6-9)** as calculated by using DFT method.

Inhib. Media	IP (eV)	EA (eV)	(eV)	(eV)	S (eV)	ω (eV)	
(6)							
Vacuum	6.568	3.471	1.548	5.019	0.645	8.139	0.639
ETOH	6.738	3.141	1.798	4.939	0.556	6.783	0.572
DMSO	6.744	3.132	1.806	4.938	0.553	6.751	0.570
H$_2$O	6.747	3.128	1.809	4.938	0.552	6.737	0.569
(7)							
Vacuum	6.740	3.170	1.785	4.955	0.560	6.878	0.572
ETOH	6.963	3.147	1.907	5.055	0.524	6.698	0.509
DMSO	6.964	3.149	1.907	5.057	0.524	6.704	0.509
H$_2$O	6.984	3.151	1.916	5.067	0.521	6.699	0.503
(8)							
Vacuum	0.637	3.773	1.417	5.191	0.705	9.504	0.637
ETOH	0.565	3.425	1.677	5.103	0.596	7.763	0.565
DMSO	0.563	3.418	1.683	5.102	0.593	7.729	0.563
H$_2$O	0.562	3.414	1.687	5.101	0.592	7.713	0.562
(9)							
Vacuum	6.328	3.207	1.560	4.767	0.640	7.284	0.715
ETOH	6.477	3.172	1.652	4.825	0.605	7.044	0.657
DMSO	6.486	3.174	1.655	4.830	0.603	7.044	0.655
H$_2$O	6.489	3.175	1.657	4.832	0.603	7.044	0.653

Active sites of the compound (7)

The inhibition of the investigated inhibitor was done through its reactive centers (nucleophilic and electrophilic centers) using Mulliken charges population analysis. Table 8 shows that the oxygen, nitrogen and some carbon atoms have the higher negative charge, whereas C4 atom has high electron density (-0.540). Destinations for nucleophilic reactive sites of compound **(7)** were O13, N17, N18,

O22 and the carbon atoms which have negative charge could be considered as an active adsorption center towards the metal surface.

The nucleophilic and electrophilic electronic charge values of compound **(7)** show that they are stronger in ETOH, DMSO and H_2O solution than that in the vacuum making among adsorption by donating electrons.

Table-7 shows that the nucleophilic reactive sites are N18< N17< C15< C7< O13< C4< C9 and the electrophilic reactive sites are C2< C16< C19< C3< C8**.**

Table 7-DFT Mulliken charges population analysis for the calculated inhibitor molecule compound (7) in media (vacuum, ETOH, DMSO, and H_2O).

Atom	Electronic Charge (ecu)	Atom	Electronic Charge (ecu)	Atom	Electronic charge (ecu)
N1	-0.178V -0.166E -0.166D -0.165W	C9	-0.535V -0.594W -0.591E -0.593D	N17	-0.295V -0.343W -0.341E -0.343D
C2	0.194V 0.248E 0.250D 0.251W	N10	0.023V 0.076E 0.078D 0.079W	N18	-0.194V -0.298E -0.303D -0.303W
C3	0.559V 0.617E 0.619D 0.620W	O11	-0.135V -0.195E -0.198D -0.199W	C19	0.396V 0.439E 0.441D 0.442W
C4	-0.540V -0.513E -0.512D -0.512W	O12	-0.158V -0.208E -0.210D -0.211W	N20	-0.124V -0.081E -0.080D -0.079W
C5	-0.021V -0.049E -0.049D -0.049W	O13	-0.456V -0.493E -0.494D -0.495W	C21	0.111V 0.101E 0.100D 0.100W
C6	0.190V 0.218E 0.219D 0.219W	N14	-0.077V -0.153E -0.156D -0.158W	O22	-0.401V -0.418E -0.419D -0.419W
C7	-0.434V -0.453E -0.453D -0.454W	C15	-0.317V -0.339E -0.341D -0.341W	------	------
C8	0.001V 0.805E 0.805D 0.804W	C16	0.281V 0.330E 0.332D 0.333W	------	------

V: vacuum phase, D: dimethyl sulfoxide (DMSO), W: water, blue color: increase in electronic charge to more positive, red color: increase in electronic charge to more negative, ecu = electron control unit.

Corrosion inhibition measurement

Potentiodynamic polarization curves and Corrosion kinetic

The electrochemical corrosion parameters are presented in Table 9 such as corrosion potential (E_{corr}), Tafel slopes (bc, ba) and corrosion current density (I_{corr}) obtained by of cathodic and anodic regions of the Tafel lines. Figure-3 presents potentiodynamic polarization curves for C.S in sea water containing different conditions of compound (7). IE%, Ө, can be measured using the following Equations:

$$\%IE = (I_{corr\,(uninh)} - I_{corr\,(inh)} / I_{corr\,(uninh)}) \times 100 \qquad (10)$$

$$\Theta = (I_{corr\,(uninh)} - I_{corr\,(inh)} / I_{corr\,(uninh)}) \qquad (11)$$

Where $I_{corr\,(inh)}$ is the inhibited corrosion current densities, $I_{corr\,(uninh)}$ is the uninhibited current densities.

Table-8 showing the decreasing in IE% with the increase in temperature which may be indicating a physisorption inhibition process [18]

Table 8-Electrochemical data of the C.S corrosion in sea water at different concentrations for compound (7).

| Inhibitor Conc. (mg/ L)	T/ K	E_{corr} (mV)	I_{corr} (μAcm^{-2})	b_c (mV dec^{-1})	b_a (mV dec^{-1})	IE%	Θ
Blank	298	-621.0	121.69	-146.9	82.1	-	-
	308	-785.7	164.53	-26.3	73.8	-	-
	318	-608.0	191.16	-102.0	315.2	-	-
5	298	623.5	20.35	-	44.0	83.277	0.833
	308	-547.3	29.44	-256.3	75.7	82.107	0.821
	318	579.4	37.95	-146.6	78.7	80.148	0.801
10	298	623.0	18.96	-275.0	73.9	84.419	0.844
	308	588.3	26.02	-131.9	75.4	84.185	0.841
	318	595.1	36.64	-171.2	92.0	80.832	0.808
20	298	-537.2	15.69	-110.1	72.5	87.106	0.871
	308	-484.2	23.84	-391.8	69.0	85.510	0.855
	318	-528.2	31.26	-263.5	88.2	83.647	0.836
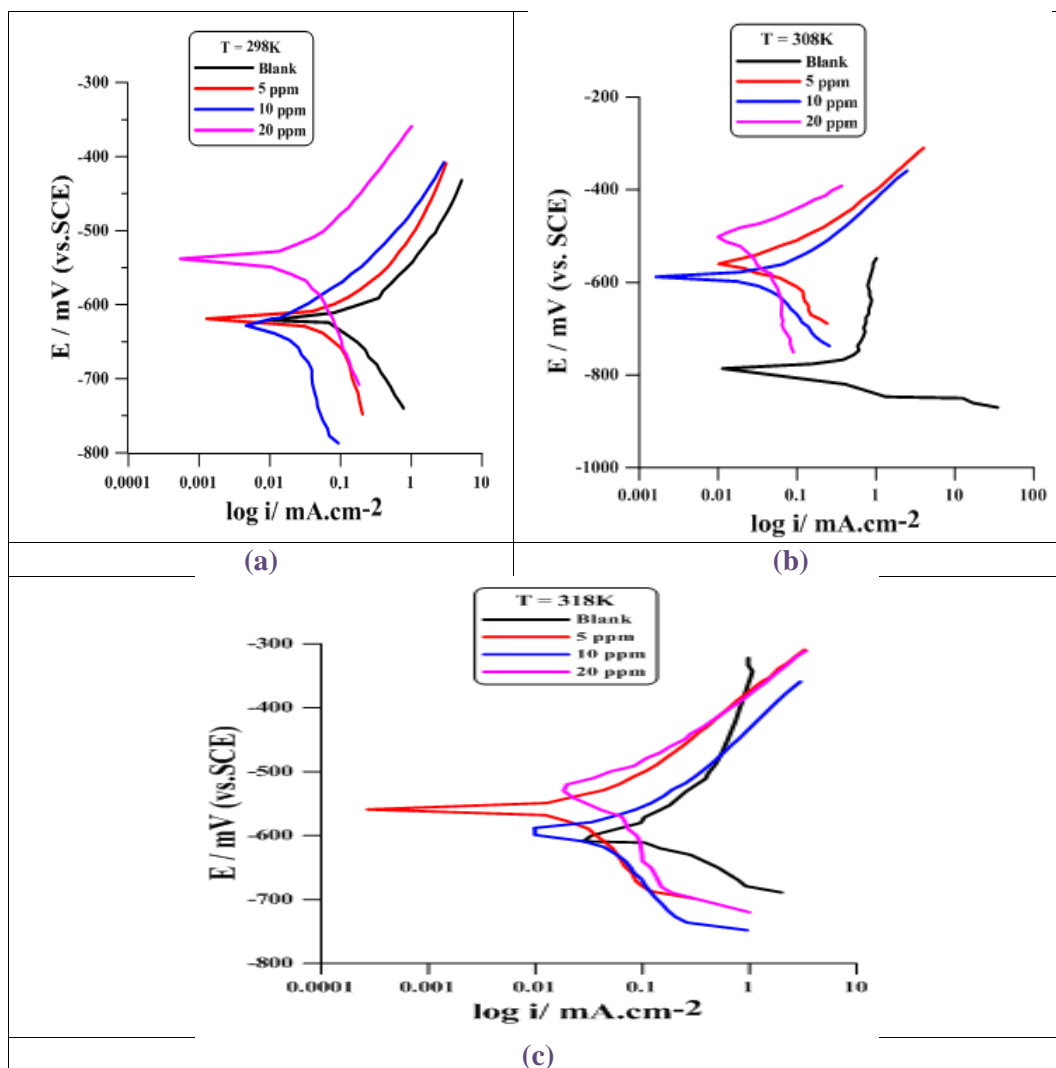
Figure 3-olarization curve of C.S in sea water for different concentrations of compound (**7**) at temperature (a) 293K, (b) 308K, (c) 318 K.

Thermodynamic and activation parameters

The Arrhenius law presented as a straight line of the logarithm of the corrosion rate. The linear regression plots between log I_{corr} and $1/T$ are presented in Figure-4.The activation energy of the corrosion process (Ea), and the pre-exponential factor (A), are calculating from Equations 12 and 13.

Log (I_{corr}) = Log A – Ea /2.303RT   (12)

Log (I_{corr}/T) = Log (R/Nh) + ΔS*/2.303R - ΔH*/2.303RT   (13)

Where (I_{corr}) is the corrosion current density, (R) is the universal gas constant (8.314 J mol^{-1} K^{-1}), (T) is temperature in K, (h) is the Plank's constant (6.626 x 10^{-34} J s), (N) is the Avogadro's number (6.022 x 10^{23} mol^{-1}), ΔH is the enthalpy of activation and ΔS is the entropy of activation.

A plot of log (I_{corr}/ T) against (1/ T) gave linear relationship with a slope of (−ΔH*/ 2.303R) and an intercept of [log(R/ Nh)+ (ΔS*/ 2.303R)] as shown in Figure-5, from which the activation thermodynamic parameters (ΔH* and ΔS*) were calculated, Table-9.

The enthalpy changes (ΔH*) of the corrosion reaction in 3.5% NaCl at a temperature range of (298-318) K have positive values indicating an endothermic nature for this reaction [19]. The lower negative values of entropy (ΔS*) obtained for corrosion processes meaning a decrease in the degree of freedom and a consequent restriction of the corrosion process [20].

The values of ΔG of corrosion processes were calculated from the following relation:

ΔG* = ΔH*-T ΔS*   (14)

Table 9-Corrosion kinetic parameters for carbon steel in sea water (3.5% NaCl) for blank within various concentrations of the inhibitor.

Conc. (mg/ L)	ΔG/ kJ mol^{-1}			ΔH* kJ mol^{-1}	ΔS* kJ mol^{-1} K^{-1}	Ea kJ mol^{-1}	A Molecules cm^{-2} S^{-1}
	298K	**308K**	**318K**				
Blank	61.037	62.572	64.107	15.293	-0.154	17.853	1.006E+29
5	65.469	66.927	68.385	22.019	-0.146	24.585	2.53861E+29
10	65.722	67.143	68.564	23.379	-0.142	25.925	3.97737E+29
20	66.107	67.498	68.890	24.642	-0.139	27.208	5.65713E+29

y = -932.4x + 5.223
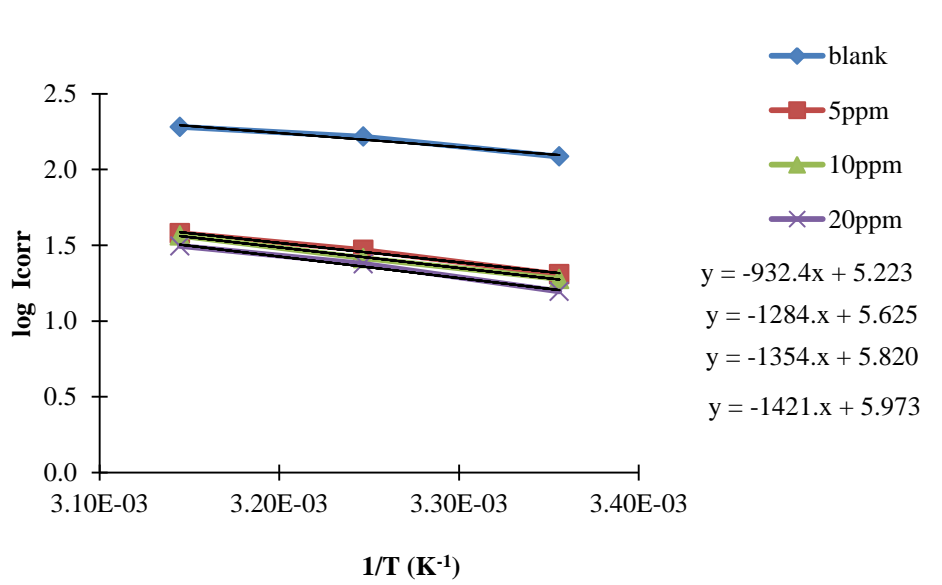y = -1284.x + 5.625
y = -1354.x + 5.820
y = -1421.x + 5.973

Figure 4-Plot of log I_{corr} vs (1/T) for the corrosion for carbon steel in sea water (3.5% NaCl) containing different concentrations of the inhibitor
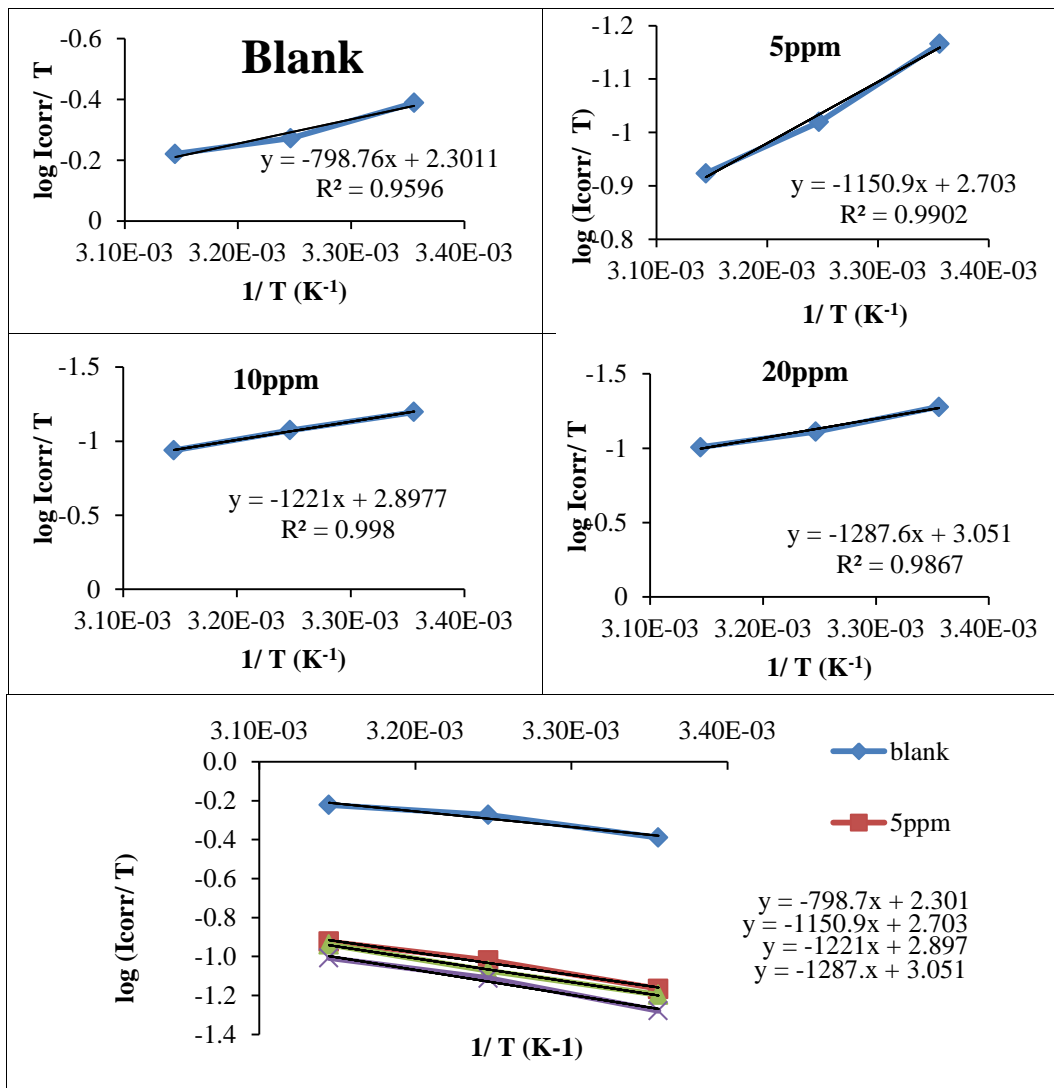
Figure 5-Plot log (I_{corr}/ T) vs (1/T) of carbon steel in sea water for blank and in presence different concentrations of the inhibitor.

Adsorption isotherm

The adsorption isotherms are useful to describe the reaction between the inhibitor molecules with carbon steel surface.

Langmuir adsorption isotherm can be represented by the following equation [21].

$$C/\Theta = (1/K_{ads}) + C \qquad (15)$$

Whereas C is the inhibitor concentration, K_{ads} is the adsorption/ desorption equilibrium constant. A plot of C/θ versus C, could be used to determine the equilibrium adsorption constant K_{ads}, then the thermodynamic functions, Figure-6. For the adsorption process, these functions are (ΔH_{ads}, ΔS_{ads} and ΔG_{ads}) represent in Table 10. ΔG_{ads} was calculated using Equation 16 [22].

$$\Delta G_{ads} = -2.303 \, RT \, Log \, (55.55 K_{ads}) \qquad (16)$$

Whereas R: is the gas constant (J K^{-1} mol^{-1}), T: is the absolute temperature (K), and 55.5: is the molar concentration (mol L^{-1}) of water in the solution. By plotting K_{ads} versus (1/T) the $\Delta G°_{ads}$ was extracted from the slope entropy and enthalpy adsorption values by using Equations 17, 18, Figure-7.

$$\Delta G°_{ads} = -RT \ln K_{ads}. \qquad (17)$$

$$\Delta G°_{ads} = \Delta H°_{ads} - T\Delta S°_{ads} \qquad (18)$$

Negative values of the $\Delta G°_{ads}$ reflect the spontaneous adsorption. In general, values of $\Delta G°_{ads}$ around or below (-40 kJ mol^{-1}) are compatible with physisorpti on and those around or more negative than (-40 kJ mol^{-1}) involve chemisorptions [23]. The calculated values for $\Delta G°_{ads}$ have been found in the range of (-11.815 to -12.672 kJ mol^{-1}) at different temperatures (298-318 K). These values fall between the threshold values for the physisorption.

The entropy $\Delta S°_{ads}$ value was positive confirming that the corrosion process is entropically favorable [24]. The negative value of $\Delta H°_{ads}$ indicates the adsorption of inhibitory molecules on the C.S surface is an exothermic process. For compound (**7**) $\Delta H°_{ads}$ is equal to (-13.717 kJ mol^{-1}) [25].

Table 10-Thermodynamic parameters for adsorption of compound (**7**) on C.S surface in 3.5% NaCl at various temperatures

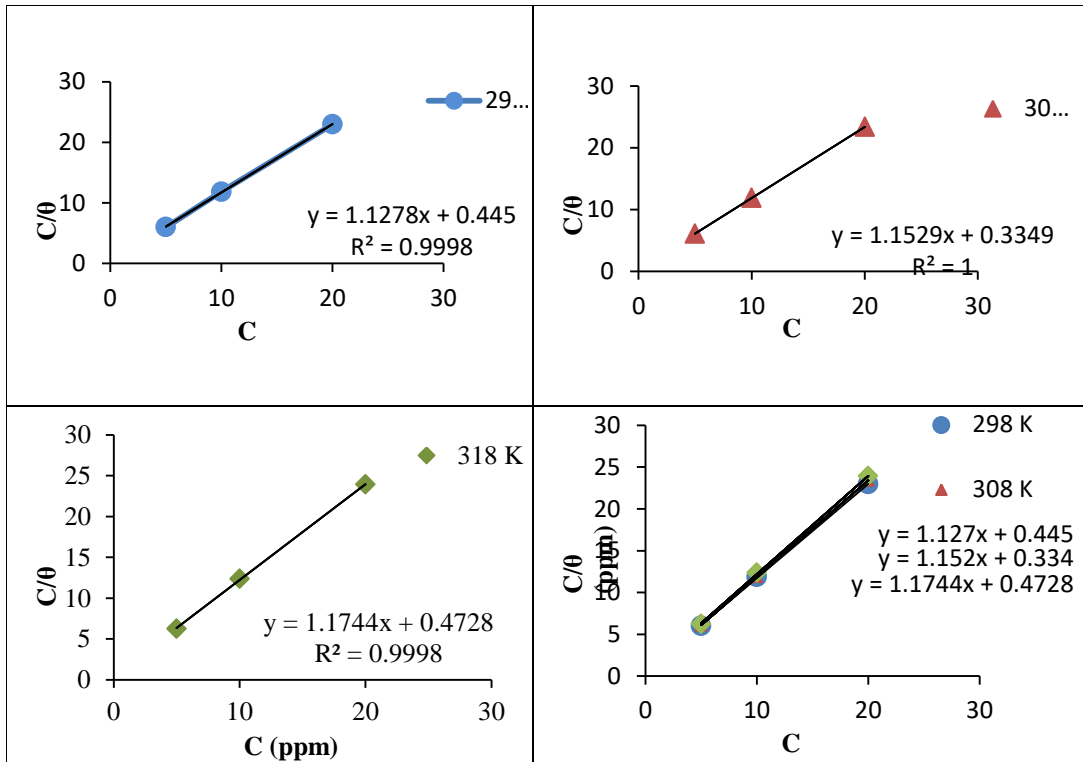| T/ K	K_{ads}	ΔG kJ mol^{-1}	R^2	ΔH_{ads} kJ mol^{-1}	ΔS_{ads} kJ mol^{-1} K^{-1}
298	2.99401	-12.672	0.999		
308	2.24719	-11.961	1.000	-13.7170	0.0038
318	2.11864	-11.815	0.999		

Figure 6- angmuir isotherms plots for the adsorption of compound (**7**) on carbon steel at the temperature range of (298, 308 and 318) K.
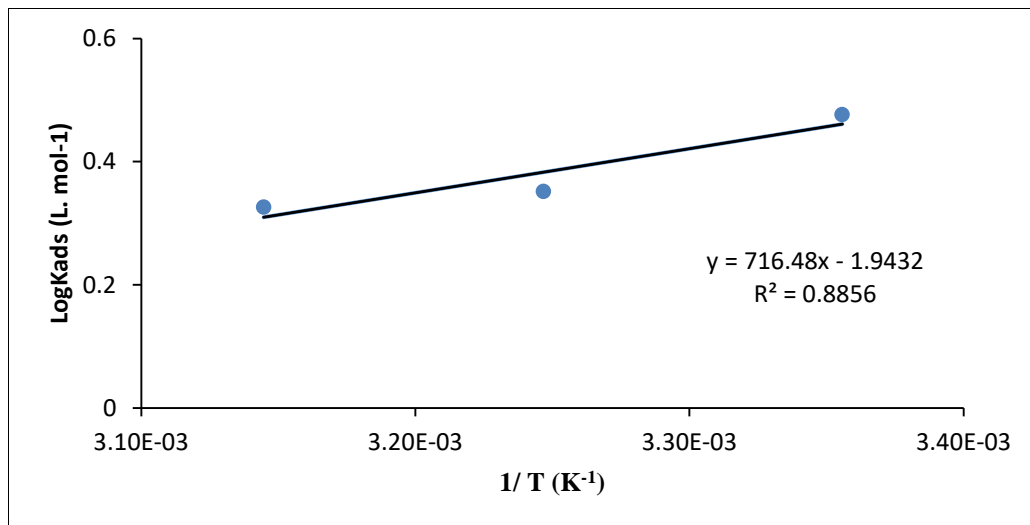

Figure 7-Plot of log K_{ads} vs (1/T) for compound (**7**)

Scanning Electron Microscopy (SEM)

In Figure-8a, the badly damaged surface obtained when the metal was remained immersed in saline water. However, Figure-8b shown C.S surface in the presence of inhibitor(7) has respected smoothness as compared to Figure-8a, indicating reduction of the corrosion rate. This improvement in surface morphology is due to the formation of a protective film of compound (7) inhibitor on the C.S surface which is represent for inhibition of corrosion [26].
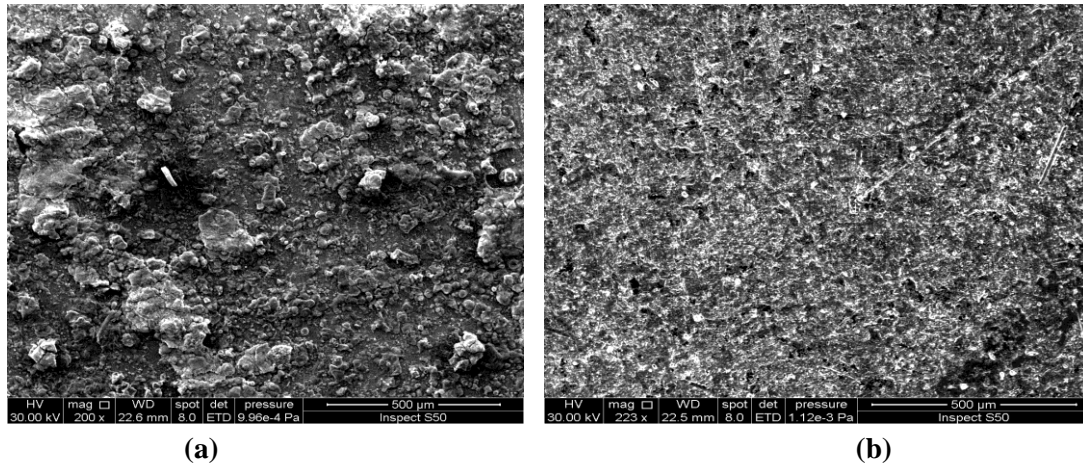

(a)	**(b)**

Figure 8-SEM images of carbon steel in a 3.5% NaCl solution immersion at 298 K (a) without inhibitor (b) in presence of compound **(7)** inhibitor**.**

Atomic force microscopy

Surface morphology of carbon steel sample in a 3.5% NaCl solution in the absence and presence of inhibitor (7) was investigated by atomic force microscopy (AFM). The results are shown in Figure 9(a–f). The average roughness is clearly shown in Figure-9 (a, b and c) that carbon steel sample is badly damaged due to the 3.5% NaCl salt attack on the surface. The average roughness value (Sa), root mean square value; Sa (mean roughness value (Sq), peak valley height (Sy) for the carbon steel surface 2.79 nm, 4.11 nm, and 42.8 nm, respectively. However, in the presence of an optimum concentration (20 ppm) of compound (3) as shown in Figure-9(d, e and f), the average roughness was reduced that display the steel surface after immersion in 3.5% NaCl solution presence of inhibitor. The (Sa), (Sq), (Sy) for the carbon steel surface are 47 nm, 60.9 nm, and 315 nm, respectively [27].

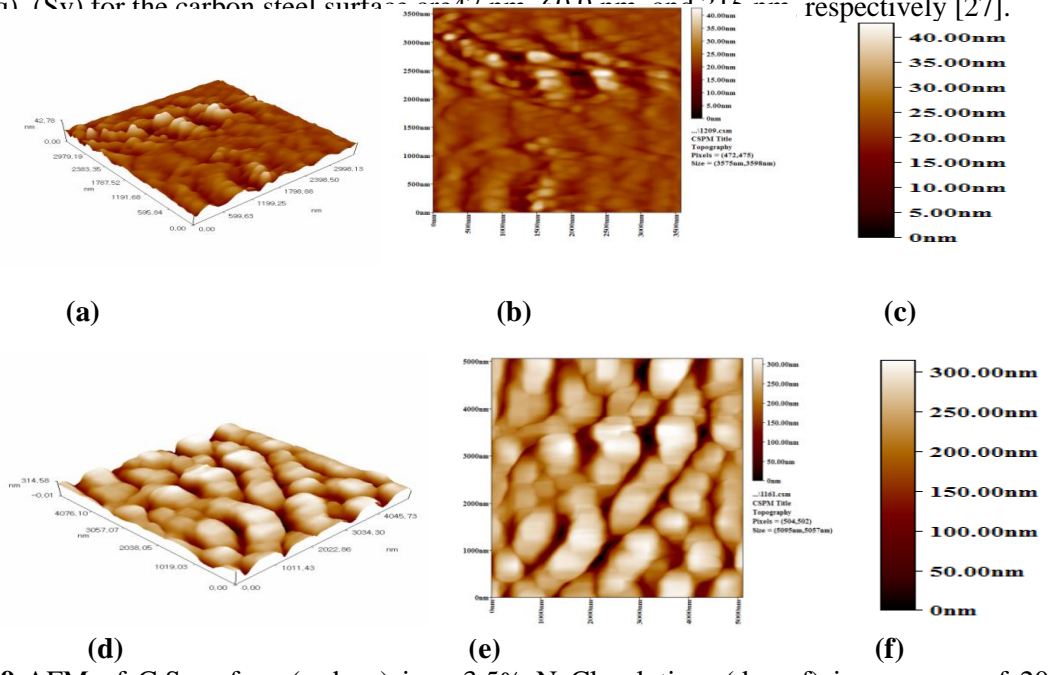|		
(a)	**(b)**	**(c)**
(d)	**(e)**	**(f)**

Figure 9-AFM of C.S surface (a, b, c) in a 3.5% NaCl solution, (d, e, f) in presence of 20 ppm compound (7).

Conclusions
1. The new synthesized isatin semicarbazides and 1, 2, 4-triazole derivatives (2-9), were theoretically to be as an organic corrosion inhibitors for carbon steel. The best one was compound (7).
2. The inhibition efficiency obtained for compound (7) using potentiodynamic polarization measurements reflected that the studied inhibitor could be classified as a mixed inhibitor in 3.5% NaCl.
3. The inhibition efficiency increased with increasing inhibitor concentration and decreased with increasing temperature.
4. The adsorptions of the studied compound on C-steel follow the Langmuir adsorption isotherm model. The low K_{ads} values indicate a physical reaction between the inhibitor and the metal surface, and the ($\Delta G°_{ads}$) values suggest also that this interaction may occur by physical adsorption.

References
1. Zhenzhen, X., Guangcheng, W., Jing, W., Ming, C., Yaping, P., Luyao, L., Bing, D., Shan, C. and Wenbiao, L. **2017**.Synthesis, biological evaluation, and molecular docking studies of novel isatin-thiazole derivatives as α-glucosidase inhibitors. *Molecules*, **22**(659): 1-11.
2. Ghochikyan, T., Samvelyan, M., Galstyan, A. and Grigoryan, S. **2016**. Synthesis of some of s-derivatives of 1,2,4-triazoles, *Proc. of the Yerevan State Univ. Chemistry and Biology*. **2**: 8–12.
3. El Bakri, Y., Boudalia, M., Echihi, S., Harmaoui, A., Sebhaoui, J., Elmsellem, H., Ramli, Y., Guenbour, A., Bellaouchou, A. and Essassi, E.**2017**.Performance and theoretical study on corrosion inhibition of new Triazolopyrimidine derivative for Carbon steel in hydrochloric acid. *Journal of materials and Environmental Sciences*, **8**(2): 378-388.
4. David, A. **2017**. Predicting the performance of organic corrosion inhibitors. *Metals*, **7**(553): 1-8.
5. Aouniti, A., Elmsellema, H., Tighadouini, S., Elazzouzi, M., Radi, S., Chetouani, A., Hammouti, B. and Zarrouk, A. **2016**. Schiff's base derived from 2-acetyl thiophene as corrosion inhibitor of steel in acidic medium.*Journal of Taibah University for Science*, **10**: 774-785.
6. Mohammed, G. and Suaad, M. **2014**. Synthesis, characterization and evaluation antimicrobial activity of some new substituted 2-mercapto-3-phenyl-4(3H)- quinazolinone, *Iraq. J. Sci.*, **55**(2): 582-593.
7. Rehab, M.K., Suaad, M., Athraa, H. **2018**. Synthesis, identification, theoretical and experimental studies for carbon steel corrosion inhibition in sea water for new urea and thiourea derivatives linkage to 5-nitro isatin moiety, *Der Pharma Chemica,* 10(7): 86-99.
8. Hasan, S. **2008.** Synthesis and identification of five, six and seven membered ring heterocyclic derivatives, M.Sc. Thesis, Al-Nahrain University, collage of Science, p 67.
9. Sahar, B. **2007**. Synthesis of new heterocyclic compounds derived from phenyl acetic acid and study of biological activity for some of these compounds, M.Sc. Thesis, College of Science, Al-Nahrain University, p 155.
10. Ayad, K. **2013**. Synthesis and characterization of new heterocyclic derivatives from 1,8-naphthalic anhydride and studying their applications as antimicrobial agents, Ph.D. Thesis, College of Science, University of Baghdad, p 131.
11. Rajendran, M., Keerthika, K., Kowsalya, M. and Devapiriam, D. **2016**. Theoretical studies on corrosion inhibition efficiency of pyridine carbonyl derivatives using DFT method.*Der Pharma Chemica*, **8**(3): 71-79.
12. Frisch, M., Trucks, W., Schlege, G., Scuseria, H., Robb, G., Cheeseman, M., Montgomery, J., Vreven, J., Kudin, T. Burant, K. Millam, J. Iyengar, J. Tomasi, S. Barone, J. Mennucci, V. Cossi, B. Scalmani, M., Rega, G., Petersson, N., Nakatsuji, G., Hada, H., Ehara, M., Toyota, M., Fukuda, K., Hasegawa, R., Ishida, J., Nakajima, M., Honda, T., Kitao, Y., Nakai, O., Klene, H., Li, M., Knox, X., Hratchian, J., Cross, H., Bakken, J., Adamo, V., Jaramillo, C., Gomperts, J., Stratmann, R., Yazyev, R., Austin, O., Cammi, A., Pomelli, R., Ochterski, C., Ayala, J., Morokuma, P., Voth, K., Salvador, G., Dannenberg, P., Zakrzewski, J., Dapprich, V., Daniels, S,. Strain, A., Farkas, M., Malick, O., Rabuck, D., Raghavachari, A., Foresman, K., Ortiz, J., Cui, J., Baboul, Q., Clifford, A., Cioslowski, S., Stefanov, J.,Liu, B., Liashenko, G., Piskorz, A., Komaromi, P., Martin, I., Fox, R., Keith, D., Al-Laham, T., Peng, M., Nanayakkara, C., Challacombe, A., Gill, M., Johnson, P., Chen, B., Wong, W., Gonzalez, M. and Pople, J. Gaussian 03, Gaussian. Inc. Pittsburgh PA, **2009**.

13. Becke, A. **1993**. Density-functional thermochemistry. III. The role of exact exchange.*Journal of Chemestry and Physical*, **98**: 5648-5652.
14. Ee, C., Yang, W. and Parr, R. **1988**. Development of the colle-salvetti correlation-energyformula into a functional of the electron density.*Physical Review,* B 41: 785-789.
15. Rehab, M.K. and Mustafa, M.K. **2016**.Theoretical studies of corrosion inhibition efficiency of two new N-phenyl-ethylidene-5-bromo isatin derivatives. *Iraqi Journal of Science*, 57(2B): 1041-1051.
16. Raafat, M., Mohamed, K. and Faten, M. **2008**. Quantum chemical studies on the inhibition of corrosion of copper surface by substituted uracils. *Applied Surface Science*, **255**: 2433-2441.
17. Henriquez-Román, J., Sancy, M., Páez, M., Padilla-Campos, L., Zagal, J., Rangel, C. and Thompson, G. **2005**. The influence of aniline and its derivatives on the corrosion behaviour of copper in acid solution. *Journal of Solid State Electrochemistry*, **9**(7): 504-511.
18. Rehab, M.K. and Fatten, K. **2015**. DFT, PM3, AM1, and MINDO/3 quantum mechanical calculations for some INHC Cs symmetry schiff bases as corrosion inhibitors for mild steel.*Iraqi Journal of Science*, **56**(1C): 602-621.
19. Ben Hmamou, D., Aouad, M., Salghi, R., Zarrouk, A., Assouag, M., Benali, O., Messali, M., Zarrok, H. and Hammouti, B. **2012**.Inhibition of C38 steel corrosion in hydrochloric acid solution by 4,5-diphenyl-1H-imidazole-2-thiol:gravimetric and temperature effects treatments. *International Journal of Science and Research,***4**(7): 3498- 3504
20. Abd-El-Naby, B., Abdullatef, O., Khamis, E. and El-Mahmody, W. **2016**.Effect of cetyltrimethylammonium bromide surfactant as novel inhibitor for the corrosion of steel in 0.5 M H_2SO_4.*International Journal Electrochemstry and Science,***11**: 1271-1281.
21. Uday, H., Suaad, M. and Khulood, A. **2013**. Corrosion inhibition effects of some new synthesized N-Aroyl-N\-Aryl thiourea derivatives for carbon steel in sulfuric acid media.*Journal of Al-Nahrain University*, **16**(4): 80-93.
22. Rehab, M.K., Dhuha, A. and Suaad, M. **2017**.Quantum mechanical and electrochemical study of new isatin derivative as corrosion inhibitor for carbon steel in 3.5 % NaCl.*International Journal of Science and Research*, **6**(7): 1656-1669.
23. Hong, S., Chen, W., Luo, H. and Li, N. **2012**. Inhibition effect of 4-amino-antipyrine on the corrosion of copper in 3 wt.% NaCl solution.*Corrosion Science,***57**: 270-278.
24. Issa, R., El-Sonbati, A., El-Bindary, A. and Kera, H. **2002**.Potentiometric and thermodynamic studies of 2-acrylamidosulfamethazine and its metal complexes. *Journal of Eurpan Polymar*, **38**: 561.
25. El-Ouali, I., Hammouti, B., Aouniti, A., Ramli, Y., Azougagh, M., Essassi, E. and Bouachrine, M. **2010**. Thermodynamic characterisation of steel corrosion in HCl in the presence of 2-phenylthieno (3, 2-b) quinoxaline. *Journal of Material and Enviromantal Science*, **1**(1): 1-8.
26. Mohamed, A., Khaled, Z., Hamdy, A., Abo-Elenien, O. and Olfat, E. **2015**. Synthesis of novel schiff base silicon compound for employing as corrosion inhibitor for carbon steel in the 1 M HCL and 3.5% NaCl aqueous media. *International Journal of Chemical, Environmental & Biological Sciences*, **3**: 2320-4087
27. Gowri, S., Sathiyabama, J., Prabhakar, P. and Rajendran, S. **2012**. Inhibition behaviour of carbon steel in sea water in the presence of tyrosine- Zn^{2+} system. *International Journal of Research in Chemistry and Environment*, **3**: 156-162.